Nano Res (2008) 1: 203–212
DOI 10.1007/s12274-008-8021-8
Research Article

Nano-Graphene Oxide for Cellular Imaging and Drug Delivery

Xiaoming Sun, Zhuang Liu, Kevin Welsher, Joshua Tucker Robinson, Andrew Goodwin, Sasa Zaric, and Hongjie Dai (✉)

Department of Chemistry and Laboratory for Advanced Materials, Stanford University, Stanford, CA 94305, USA

Received: 24 May 2008 / Revised: 1 July 2008 /Accepted: 1 July 2008

ABSTRACT

Two-dimensional graphene offers interesting electronic, thermal, and mechanical properties that are currently being explored for advanced electronics, membranes, and composites. Here we synthesize and explore the biological applications of nano-graphene oxide (NGO), i.e., single-layer graphene oxide sheets down to a few nanometers in lateral width. We develop functionalization chemistry in order to impart solubility and compatibility of NGO in biological environments. We obtain size separated pegylated NGO sheets that are soluble in buffers and serum without agglomeration. The NGO sheets are found to be photoluminescent in the visible and infrared regions. The intrinsic photoluminescence (PL) of NGO is used for live cell imaging in the near-infrared (NIR) with little background. We found that simple physisorption via π-stacking can be used for loading doxorubicin, a widely used cancer drug onto NGO functionalized with antibody for selective killing of cancer cells in vitro. Owing to its small size, intrinsic optical properties, large specific surface area, low cost, and useful non-covalent interactions with aromatic drug molecules, NGO is a promising new material for biological and medical applications.

KEYWORDS

Graphene oxide, pegylation, size separation, cellular imaging, drug delivery

Introduction

The interesting physical properties of graphene, a novel one-atom-thick two-dimensional graphitic carbon system, have led to much excitement in recent years in material science and condensed-matter physics [1–6]. Potential applications of graphene for nanoelectronics [1, 3], sensors, and nanocomposites [4, 5] have been actively pursued [6]. The biological applications of graphene and graphene oxide (GO) remain unexplored and wide-open, however. There are several prerequisites for biological applications for a new material. First, rational functionalization chemistry is needed to impart graphene with aqueous solubility and biocompatibility. GO and its chemically converted derivatives form stable suspensions in pure water but generally aggregate in salt or other biological solutions [6]. Second, graphene sheets with suitable sizes are desired. Size control or size separation on various length scales is necessary to suitably interface with biological systems in vitro or in vivo. Graphene and GO samples obtained thus far are typically microns or larger in size. Lastly, little is known experimentally about the properties of graphene with molecular dimensions, on the order of

Address correspondence to hdai@stanford.edu

~10 nm or below. The optical properties of graphene and GO, a topic of fundamental interest, are largely unexplored and could facilitate biological and medical research such as imaging.

Here, we report the preparation of ultrasmall nano-graphene oxide (NGO) with lateral dimensions down to <10 nm. We imparted aqueous stability to the NGO in buffer solutions and other biological media by covalently grafting polyethylene glycol (PEG) star-polymers onto the chemically activated surfaces and edges. A rate separation method was developed in order to separate the pegylated NGO according to physical dimension or size. Interestingly, the NGO sheets showed photoluminescence from visible to the near-infrared (NIR) range, which was used for cellular imaging with little background. Furthermore, an aromatic anticancer drug doxorubicin was loaded onto the NGO sheets at a high capacity via simple physisorption. The drug was selectively shuttled into cancer cells by antibody-conjugated NGO for selective killing of cancer cells.

1. Results and discussion

Our preparation of ultrasmall graphene sheets started from graphene oxide (GO) made by using a modified Hummers method (Fig. 1(a), see Method) [4–7]. Briefly, expandable graphite (Graftech Inc.) was used as starting material instead of graphite flakes to ensure more uniform oxidization [3, 8]. The graphite powder was ground with NaCl salt crystals to reduce the particle size, and then soaked in sulfuric acid for 8 h to effect intercalation. Addition of $KMnO_4$ as oxidizing agent, increasing the oxidation temperature and extending the oxidation time to ~2 h afforded fully and uniformly oxidized graphite (see Electronic Supplementary Material, ESM). The products were washed with dilute acid and water. After sonication for 1 h, the resulting GO particles were mostly single layered (> 70%, topographic height ~1.0 nm) and 10–300 nm in lateral width (Fig. 1(b)) according to atomic force microscopy (AFM) characterization. Previous work has also attributed ~1.0 nm thick GO to single-layered structures [3, 4, 6].

Infrared (IR) spectroscopy revealed the existence of –OH (~3400 cm^{-1}), C=O (1715 cm^{-1}), and C=C (1580 cm^{-1})

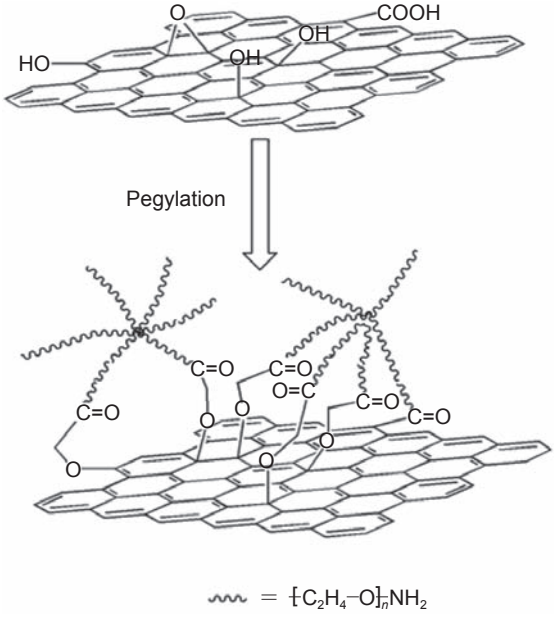

(a)

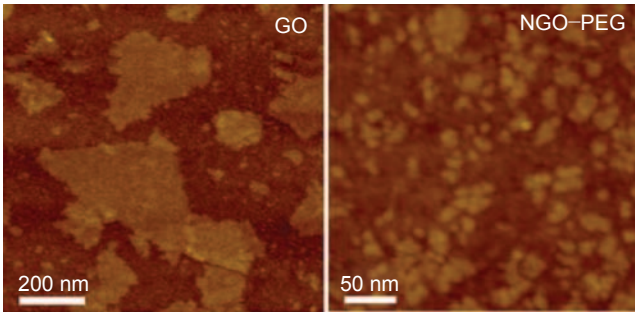

(b) (c)

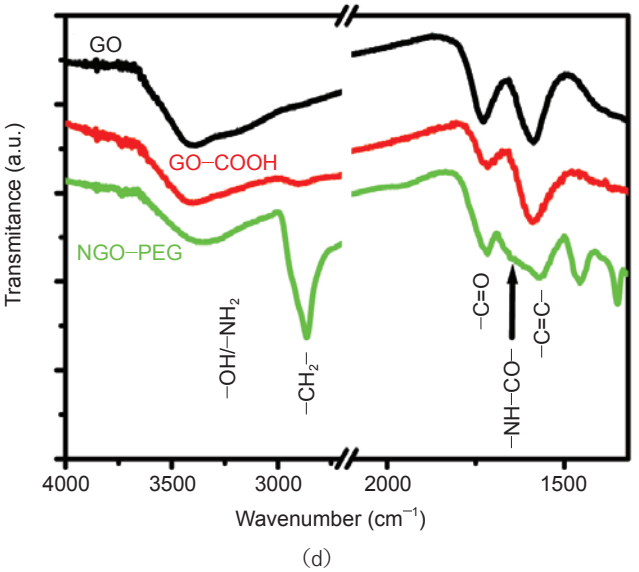

(d)

Figure 1 Synthesis and pegylation of nano-graphene oxide. (a) Schematic illustration of pegylation of graphene oxide by PEG–stars. (b), (c) AFM images of GO and NGO–PEG, respectively. (d) IR spectra of GO, GO–COOH, and NGO–PEG (the black arrow indicates the characteristic amide-carbonyl vibration)

[9, 10] functional groups in the GO (Fig. 1(d)). We activated the GO sample with chloroacetic acid under strongly basic conditions in order to activate epoxide and ester groups, and to convert hydroxyl groups to carboxylic acid (–COOH) moieties [11]. The intermediate product, named GO–COOH, had increased water solubility and more carboxylic acid groups available for subsequent pegylation (see Method). Upon grafting PEG stars (6-arm branched PEG molecules) onto the –COOH groups, we obtained a product (NGO–PEG) with high solubility and stability in salt and cellular solutions, which is desirable for biological applications. Without pegylation, GO, and GO–COOH suspensions immediately aggregated in salt and other biological solutions. AFM observed sheet sizes of mostly < 20 nm in NGO–PEG (Fig. 1(c)), while the as-made GO sheets were 10–300 nm in size (Fig. 1(b)). The ultra-small size of the NGO was caused by the sonication involved in both GO–COOH synthesis and pegylation steps. IR characterization of carefully purified NGO–PEG samples indicated strong $–CH_2–$ (2870 cm^{-1}) vibrations due to PEG chains, and a characteristic amide-carbonyl (–NH–CO–) stretching vibration (~1650 cm^{-1}, labeled with an arrow in Fig. 1(d)) [12], consistent with the grafting of PEG molecules onto NGO sheets.

Activation and pegylation of GO led to increases in optical absorption in the visible and near-infrared (vis-NIR) range for the same starting graphitic carbon mass concentration (0.01 mg/mL, Fig. 2(a)). The optical absorption peak at 230 nm, originating from the π-plasmon of carbon [13, 14], remained essentially unchanged. GO–COOH and NGO–PEG showed much higher absorbance in the vis–NIR range than GO. At 500 nm, 808 nm, and 1200 nm, the absorbance of GO–COOH and NGO–PEG were 480%, 780%, and 470% that of GO, respectively. The significant increase in absorbance led to a solution color change (darkening), visible to the eye (Fig. 2(a) inset). Similar darkening was observed in the hydrazine reduction of graphene oxide, and attributed to restoration of the electronic conjugation within the graphene sheets [4, 6]. Here, we attribute the restoration to opening of epoxide groups and hydrolysis of esters on the GO under the basic conditions employed during the activation treatment. This led to local changes in the microstructure of NGO with released local strain and increased conjugation in the GO sheets, causing increased optical absorption in the vis–NIR range.

The yellow brown color of our NGO solutions prompted us to investigate the photoluminescence of this material. Fluorescence measurements in the visible range revealed that the GO emission peaked at ~570 nm at 400 nm excitation (Fig. 2(b)). The emission maximum was blue-shifted to ~520 nm for NGO–PEG (Fig. 2(b)). Chemical activation and pegylation steps reduced the GO sheet size and changed the chemical functional groups on the sheets, which might be responsible for such a shift. We probed the IR and NIR regions and discovered photoluminescence (PL) of both GO and NGO–PEG in these regions (Figs. 2(c), 2(d)). Fluorescence in the NIR is useful for cellular imaging due to the minimal cellular auto-fluorescence in this region, as shown for single-walled carbon nanotubes [15, 16].

We developed a density gradient ultracentrifugation method [17, 18] to separate the NGO–PEG sheets by size (see Electronic Supplementary Material, Fig. S-1) and gained insight into the photoluminescence properties of NGO. By making use of the different sedimentation rates of different sized graphene in a density gradient, and by terminating the sedimentation at suitable time points, we captured different sized graphene sheets at different positions along the centrifuge tube (Fig. 2(e)). AFM of different fractions clearly indicated size separation of NGO–PEG sheets by our method (Figs. 2(f)–(h)). However, to our surprise, the different sized NGO sheets exhibited similar optical absorbance, PL and PL excitation (PLE) spectra (Electronic Supplementary Material, Fig. S-2), without the apparent quantum confinement effects expected due to the different physical sizes of the separated NGO sheets.

This somewhat unexpected result suggests that small, conjugated aromatic domains exist on a NGO sheet. That is, small conjugated domains with various sizes (~1–5 nm) coexist in a single, physically connected NGO sheet. Indeed, careful AFM imaging found small domain-like structures 1–5 nm in size (Electronic Supplementary Material, Fig. S-3). Separation of NGO sheets by physical size

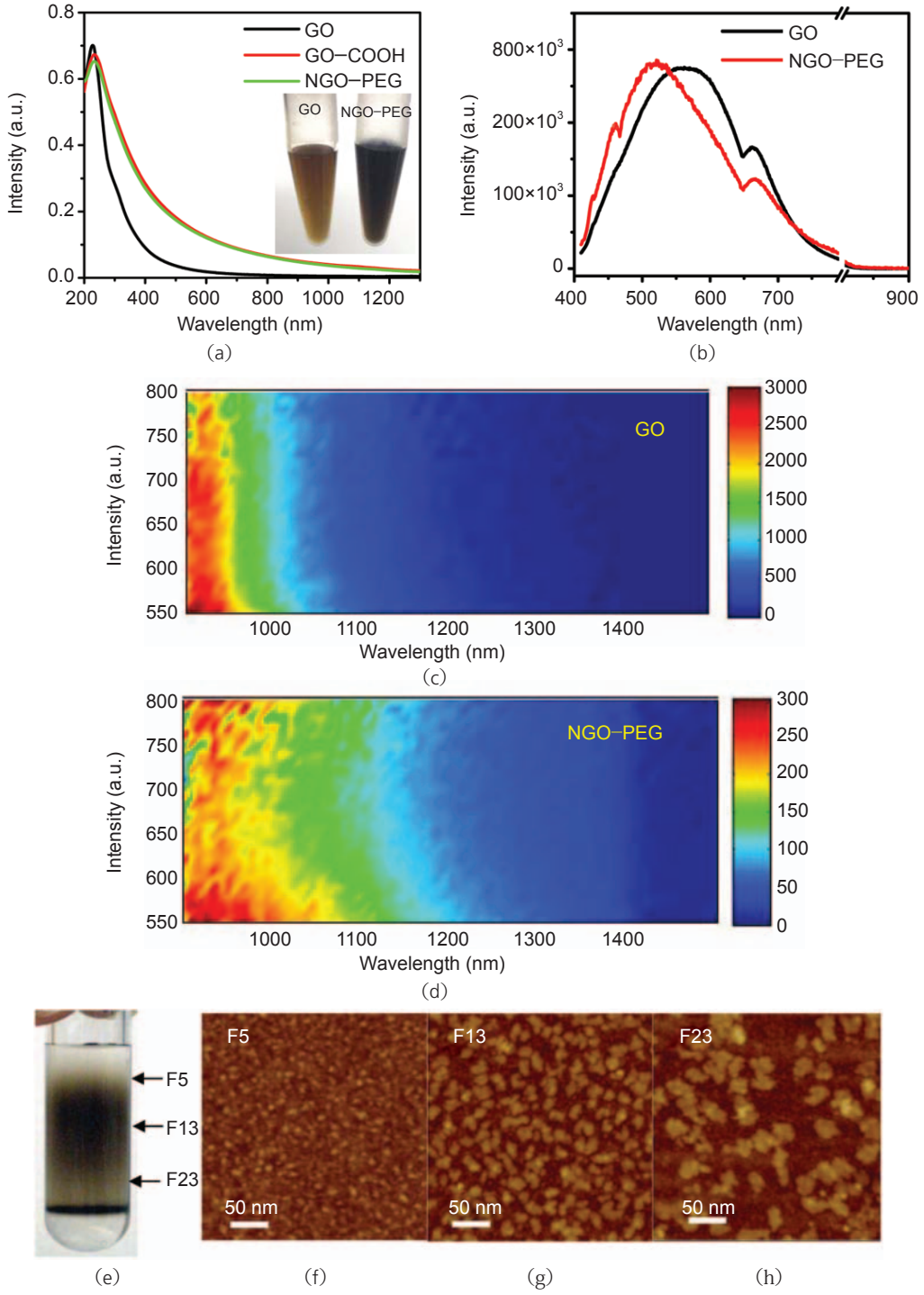

Figure 2 Optical properties of nano-graphene oxide sheets. (a) UV-vis-NIR absorbance spectra of GO, GO–COOH, and NGO–PEG solutions with 0.01 mg/mL graphitic carbon (1 cm optical path). Inset: a photograph of GO and NGO–PEG solutions at the same graphitic carbon concentration to show the visible color difference. (b) Fluorescence of GO (black curve) and NGO–PEG (red curve) in the visible range under an excitation of 400 nm. (c), (d) Photoluminescence excitation (PLE) spectra of GO & NGO–PEG with 0.31 mg/mL graphitic carbon in the IR region (1 mm optical path). The emission intensity at various emission wavelengths (*x*-axis) is represented by the color scheme shown as a function of excitation wavelength (*y*-axis). The data were obtained after normalization to detector sensitivity and absorbance curves. (e) A photograph of an ultracentrifuge tube after density gradient separation of NGO–PEG. (f)–(h) AFM images of NGO–PEG fractions (F5, F13, and F23) at different locations in the centrifuge tube as labeled in (e)

afforded various fractions exhibiting similar photoluminescence since the NGO–PEG sheets contained similar smaller aromatic domains. The domain size was inhomogeneous and ranged from small aromatic molecules to large macromolecular domains. The former was responsible for fluorescence in the visible range, while the latter gave PL in the IR range. The existence of conjugated aromatic domains spaced by non-conjugated aliphatic six-membered ring structures on GO has been shown by previous NMR experiments [19]. Nevertheless, our proposed photoluminescence mechanism is merely a suggestion, and requires further investigation. The resolution of size separation may also need significant improvement in order to observe quantum confinement effects, especially at the low end of the size distribution. It has previously been shown that after oxidative acid treatment, carbon nanoparticles (1–5 nm) exhibited fluorescence in the visible region, and that particle size and surface states significantly affected the fluorescence intensity and peak positions [20, 21]. The mechanism and chemical species responsible for this fluorescence also remain unclear [20, 21].

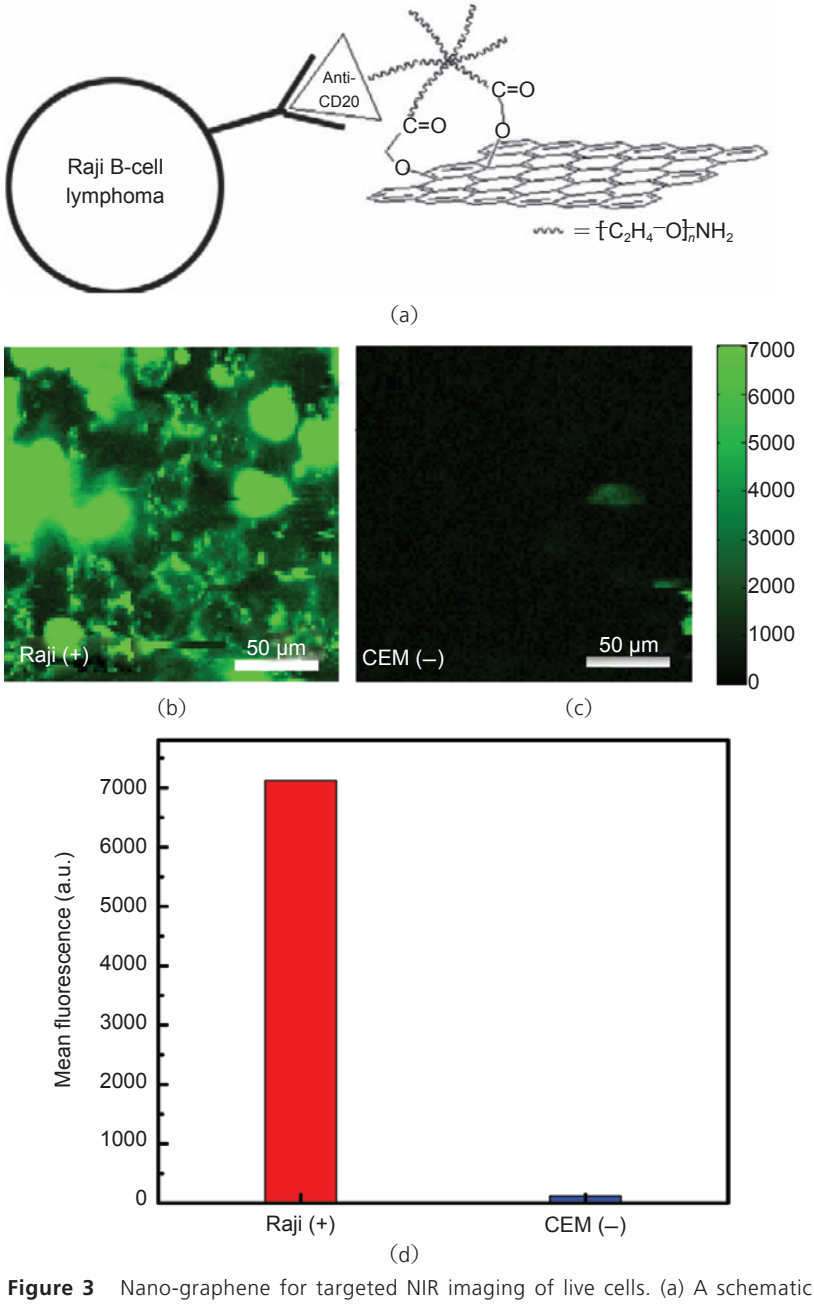

Figure 3 Nano-graphene for targeted NIR imaging of live cells. (a) A schematic drawing illustrating the selective binding and cellular imaging of NGO–PEG conjugated with anti-CD20 antibody, Rituxan. (b) NIR fluorescence image of CD20 positive Raji B-cells treated with the NGO–PEG–Rituxan conjugate. The scale bar shows the intensity of total NIR emission (in the range 1100–2200 nm). Images are false-colored green. (c) NIR fluorescence image of CD20 negative CEM T-Cells treated with NGO–PEG-Rituxan conjugate. (d) Mean NIR fluorescence intensities in the image area for the both the positive (Raji) and negative (CEM) cells treated by NGO–PEG–Rituxan conjugate

Fluorescent species in the NIR and IR range are potentially useful for biological applications since cells and tissues exhibit little auto-fluorescence in this region [16]. To this end, we covalently conjugated a B-cell specific antibody Rituxan (anti-CD20) to NGO –PEG (NGO–PEG–Rituxan) in order to selectively recognize and bind to B- cell lymphoma cells (Fig. 3(a)) [16]. We incubated B-cells and T-cells in solutions of NGO–PEG–Rituxan conjugates at 4 °C to allow the conjugates to interact with the cell surface but block internalization via endocytosis [22]. The cells were then washed and imaged by detecting NIR photoluminescence in the range 1100 to 2200 nm using a InGaAs detector under 658 nm laser excitation (laser spot size ~1 μm, see Method). We detected the intrinsic NIR photoluminescence of NGO–PEG selectively on

positive Raji B-cell surfaces (Fig. 3(b)) and not on negative CEM T-cells (Fig. 3(c)). This confirmed selective NGO–PEG–Ab binding to B-cells over T cells (Fig. 3(d)). It also established NGO as a NIR fluorophore for selective biological detections and imaging which can take advantage of the minimal cellular auto-fluorescence in the NIR region [16, 23].

The fluorescence quantum yield (QY) of the NGO–PEG was difficult to quantify due to the inhomogeneous nature of the sample. As a preliminary attempt, we compared the total emitted light by HiPCO single-walled nanotubes (SWNTs) [24–26] and NGO–PEG in the 900–1500 nm region under 785 nm excitation, and observed similar light emission (within an order of magnitude) (Electronic Supplementary Material, Fig. S-4) normalized to the same absorbance at 785 nm. Notably, for SWNTs the quantum yield issue is also not well resolved due to sample inhomogenity, and is believed to be up to several percent for certain chiralities [24, 26]. Establishing the quantum yield of graphitic nanomaterials requires significant future effort including the improvement of material homogeneity and/or separation.

Next, we explored using NGO as sheet-like vehicles to transport an aromatic drug doxorubicin (DOX), a widely used chemotherapy drug for treating various cancers, into cancer cells [27]. We first checked whether NGO–PEG exhibits any toxicity by incubating Raji cells in various concentrations of NGO–PEG for 72 h. We observed slight reductions of cell viability only for extremely high NGO–PEG concentrations (>100 mg/L) (Electronic Supplementary Material, Fig. S-5). In our subsequent cellular experiments, we used only ~2 mg/L of NGO–PEG, a concentration far below the level having any appreciable toxic effect on the cells.

Rituxan (CD20+ antibody) conjugated NGO–PEG was used to target specific cancer cells for selective cell killing (Fig. 4(a)). The loading of DOX was performed by simple mixing of an NGO–PEG–Ab solution with DOX at pH 8 overnight, followed by repeated filtering to remove free, unbound DOX in solution. The formation of NGO–PEG/DOX was visible from the reddish color of the NGO–PEG/DOX solutions due to adsorbed DOX and its characteristic UV-vis absorbance peak at 490 nm superimposed on the NGO–PEG absorption spectrum (Fig. 4(b) and inset). The loading of DOX onto NGO can be attributed to simple π-stacking, similar to that with carbon nanotubes [27]. In AFM, an obvious increase in thickness was observed as DOX was stacked onto graphene sheets (Electronic Supplementary Material, Fig. S-6). Compared to single-walled carbon nanotubes for drug loading via π-stacking [27], NGO is advantageous in terms of its low cost and ready scalability [27].

Drug release from NGO–PEG sheets was observed as the chemical environment was changed to acidic. We found that ~40% of DOX loaded on NGO–PEG was released over 1 day in an acidic solution of pH 5.5 (Fig. 4(c)), which was attributed to the increased hydrophilicity and solubility of DOX at this pH [27]. The release rate was reduced when the pH was adjusted to 7.4, being ~15% over 2 days. The pH-dependent drug release from NGO–PEG could be exploited for drug delivery applications since the micro-environments in the extracellular tissues of tumors and intracellular lysosomes and endosomes are acidic, which will afford active drug release from NGO–PEG delivery vehicles.

For DOX loaded onto NGO–PEG–Rituxan, we incubated the conjugates with Raji cells at 2 μmol/L and 10 μmol/L DOX concentrations. Enhanced DOX delivery and cell killing was evidenced by comparison with Raji cells treated with free DOX, NGO–PEG/DOX without Rituxan, and a mixture of NGO–PEG/DOX and Rituxan without covalent binding (Fig. 4(d)). It should be noted that the in vitro selectivity is limited by the passive uptake of NGO–PEG/DOX. At higher DOX concentrations, the passive uptake is high so that cells are killed by either NGO–PEG/DOX or NGO–PEG–Rituxan/DOX. However, a minimal DOX concentration is required to exhibit a biological effect. Therefore, there is a dosage window in which the selective cell killing can be achieved. This is common for many other targeted drug delivery systems. We observed very good selectivity at [DOX]=10 μmol/L. The percentage of cell growth inhibition increased from ~20% in the NGO–PEG/DOX case to ~80% in the NGO–PEG–Rituxan/DOX case, which is a significant enhancement [27]. This result

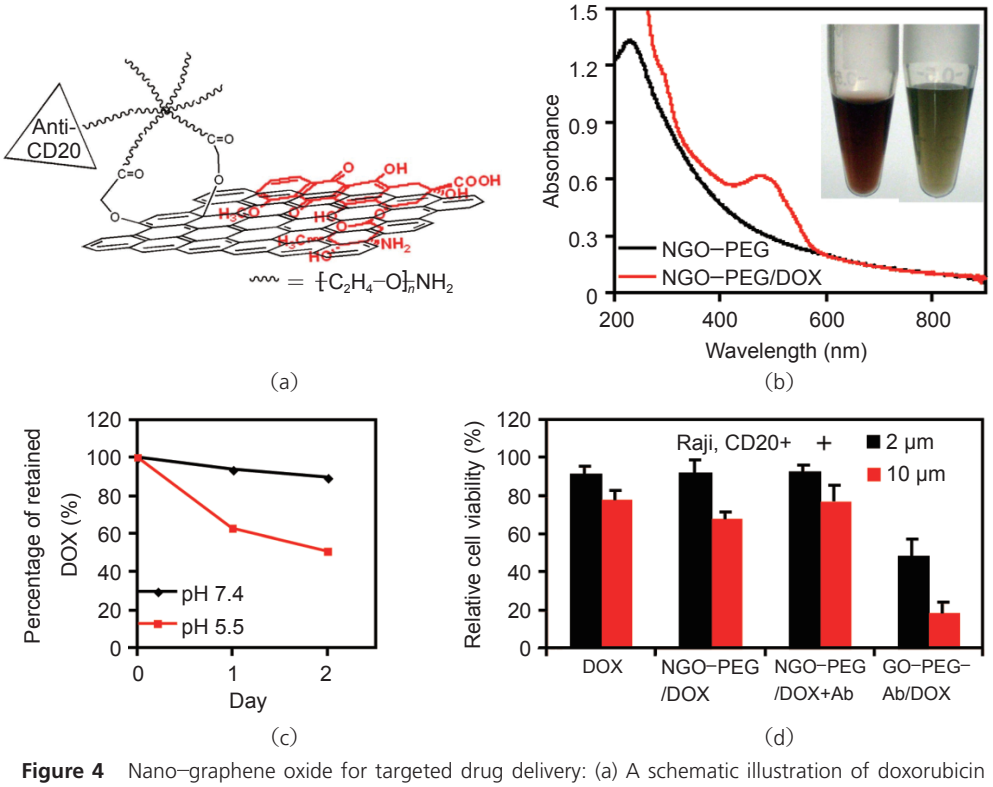

Figure 4 Nano–graphene oxide for targeted drug delivery: (a) A schematic illustration of doxorubicin (DOX) loading onto NGO–PEG–Rituxan via π-stacking; (b) UV-vis-NIR absorbance spectra of NGO–PEG and NGO–PEG/DOX. DOX loading on NGO–PEG was evidenced by a strong absorption peak centered at ~490 nm. The reddish color of the DOX loaded NGO–PEG is seen in the solution (see inset); (c) Retention of over time of DOX on NGO-PEG in buffers at pH 5.5 and 7.4; (d) In vitro toxicity test at 2 μmol/L and 10 μmol/L DOX concentration to show Rituxan selectively enhanced doxorubicin delivery into Raji B-cells by comparing NGO–PEG–Rituxan/DOX with free DOX, a mixture of DOX with NGO–PEG, and a mixture of DOX, Rituxan and NGO–PEG. The viable cell percentage was measured by the MTS assay

demonstrated the potential of selective killing of cancer cells using NGO-PEG-antibody/drug conjugates in vitro.

2. Method

2.1 Synthesis of graphene oxide

Graphene oxide (GO) was made by a modified Hummers method [7] using expandable graphite flake (Graftech) as starting material [3]. Expandable graphite flake (1 g) was ground with NaCl (50 g) for 10 min. NaCl was dissolved in water and removed by filtration (~15% carbon was lost during this step). The remaining ground expandable graphite flake (~0.85 g) was stirred in 98% H_2SO_4 (23 mL) for 8 h. $KMnO_4$ (3 g) was gradually added while keeping the temperature <20 °C. The mixture was then stirred at 35–40 °C for 30 min, and then at 65–80 °C for 45 min. Next, water (46 mL) was added and the mixture heated at 98–105 °C for 30 min. The reaction was terminated by addition of distilled water (140 mL) and 30% H_2O_2 solution (10 mL). The mixture was washed by repeated centrifugation and filtration, first with 5% HCl aqueous solution, and then distilled water. Water (160 mL) was added to the final product and vortexed well to make a uniform suspension for storage.

2.2 Pegylation of graphene oxide

For pegylation, GO aqueous suspension (5 mL) was diluted by a factor of 2 to give a concentration of ~2 mg/mL, and then bath sonicated for 1 h to give a clear solution. NaOH (1.2 g) and chloroacetic acid (Cl–CH_2–COOH) (1.0 g) were added to the GO suspension and bath sonicated for 1–3 h [11] to convert the –OH groups to –COOH via conjugation of

acetic acid moieties giving GO–COOH. The resulting GO–COOH solution was neutralized, and purified by repeated rinsing and filtrations. The GO–COOH suspension was diluted by water to give an optical density OD=0.4 at 808 nm (1 mm optical path). A solution of 6-arm polyethylene glycol-amine (Sunbio Inc.) (2 mg/mL) was added to the GO–COOH suspension and the mixture sonicated for 5 min. *N*-(3-dimethylaminopropyl-*N*′-ethylcarbodiimide) hydrochloride (EDC, from Sigma Inc.) was added in two portions to give a concentration of 4 mmol/L, allowed to react overnight, then quenched by mercaptoethanol (Fluka Inc.). The final product (NGO–PEG) was obtained by ultracentrifugation at 45000 rpm in 2× phosphate buffered saline (PBS) for 1 h, saving the supernatant (yield ~50%). The aggregates were discarded.

2.3 Separation

Rate separation in a density gradient was used for NGO–PEG separation. In a typical experiment, OptiPrep® (60% (w/v) iodixanol, 1.32 g/cm^3) (Sigma-Aldrich Inc.) was diluted with water to make 5%, 10%, 15%, and 20% iodixanol solutions. Gradients were created directly in Beckman centrifuge tubes (polycarbonate, inner diameter 13 mm, length 51 mm) by adding the four layers (0.6 mL each) to the tube bottom sequentially in order of increasing density. Finally, 60% iodixanol (0.4 mL) was added to the bottom of the centrifuge tube to raise the height of the gradient in the centrifuge tube. Freshly made NGO–6PEG (0.2 mL) was layered on top of the density gradient prior to ultracentrifugation. The typical centrifugation condition was 2.5 h at 50000 revolutions per minute (~3×10^5*g*). Calibrated micropipettors were used to manually sample 100 μL fractions along the centrifuge tube after ultracentrifugation.

2.4 Characterization

AFM was used for characterization of graphene oxide sheet size and thickness. The optical properties of graphene oxide were characterized using a ultraviolet-visible-near-infrared absorbance spectrometer (Varian Cary 6000i), fluorescence spectrometer (Spex Fluorolog 3, λ_{ex} = 400 nm) and a home built photoluminescence-excitation (PLE) spectrometer at room temperature [16].

2.5 Cellular imaging

Thiolated Rituxan was conjugated to the amine groups on NGO–PEG via a sulfosuccinimidyl 4-*N*-maleimidomethyl cyclohexane-1-carboxylate (Sulfo-SMCC) linker (Pierce Inc.) [16]. For the cell incubation, 200 μL of CEM.NK T-cell and Raji B-cell (~1 million/mL) were incubated with 50 μL of NGO–PEG with or without Rituxan conjugation in PBS for 1 h at 4 °C. The NGO–PEG concentration in the solution during incubation was ~0.7 mg/mL. Cells were washed three times with PBS to remove unbound NGO–PEG before NIR photoluminescence imaging. Cell samples prepared as described above were placed in a sample holder with a thin 200 μm quartz window. All NIR fluorescence images were taken using an inverted NIR fluorescence microscope in confocal mode. Excitation from a diode laser at 658 nm (Renishaw) was focused using a 100× IR coated objected lens (Olympus). The laser spot size width on the sample was about 1 μm FWHM. The laser intensity at the sample was ~20 mW. Emitted light was collected through the same objective and focused onto an OMA-V 1024 element linear InGaAs array (Princeton Instruments). The collected light went through a 900 nm long pass filter (Omega) and a 1100 nm long pass filter (ThorLabs) to block reflected excitation and reduce background fluorescence from the sample holder. High resolution images were taken by inserting a 50 μm pinhole in the collection path, and 1 micron steps were taken in two directions. Background fluorescence from the sample holder (~160 counts) was subtracted to give relevant statistics about the effectiveness of NGO–PEG binding.

2.6 Drug loading and cellular toxicity

Doxorubicin (DOX) loading onto NGO–PEG (and NGO–PEG–Rituxan) was done by simply mixing 0.5 mmol/L of DOX with the NGO–PEG solution (~0.2 mg/mL) at pH 8 overnight. Unbound excess DOX was removed by filtration through a 100 kDa filter and repeated rinsing. The resulting NGO–PEG/DOX complexes were re-suspended and stored at 4 °C. Concentration of DOX loaded onto NGO–

PEG was measured by the absorbance peak at 490 nm (characteristic of DOX, after subtracting the absorbance of NGO–PEG at that wavelength) with a molar extinction coefficient of 1.05×10^4 mol/(L·cm). Both Raji and CEM cells were incubated with free DOX, NGO–PEG/DOX, NGO–PEG/DOX + Rituxan (unconjugated), and NGO–PEG–Rituxan/DOX at DOX concentrations of 2 μmol/L or 10 μmol/L for 2 h and washed twice with PBS before transferring into fresh cell medium. After another 48 h incubation, cell viability was measured by the MTS assay with a CellTiter96 kit (Promega).

3. Conclusions

In summary, multifunctional biocompatible nano-graphene oxides with various physical sizes were prepared in a scalable manner. Photoluminescence of NGO from visible through infrared range was revealed and used for cellular imaging. Anticancer drugs were loaded onto NGO with high capacity, and selectively transported into specific cancer cells by antibody guided targeting. The novel graphitic nanostructures, combined with multi-functionalities including biocompatibility, photoluminescence and drug loading and delivery, suggest promising applications of graphene materials in biological and medical areas.

Acknowledgements

This work was supported by NIH-NCI funded CCNE–TR at Stanford University. We are grateful to Drs. Alice Fan and Dean Felsher for providing the antibodies used in this work.

Electronic Supplementary Material: Experimental details of synthesis, pegylation of NGO, characterization, antibody (Rituxan) conjugation, cell culture, and NIR imaging of cells can be found in the supplementary material with 6 supplementary figures. Supplementary material is available in the online version of this article at http: //dx.doi.org/DOI 10.1007/s12274-008-8021-8 and is accessible free of charge.

References

[1] Geim, A. K.; Novoselov, K. S. The rise of graphene. *Nat. Mater.* **2007**, *6*, 183–191.

[2] Kopelevich, Y.; Esquinazi, P. Graphene physics in graphite. *Adv. Mater*. **2007**, *19*, 4559–4563.

[3] Li, X.; Wang, X.; Zhang, L.; Lee, S.; Dai, H. Chemically derived, ultrasmooth graphene nanoribbon semiconductors. *Science* **2008**, *319*, 1229–1232.

[4] Stankovich, S.; Dikin, D. A.; Dommett, G. H. B.; Kohlhaas, K. M.; Zimney, E. J.; Stach, E. A.; Piner, R. D.; Nguyen, S. T.; Ruoff, R. S. Graphene-based composite materials. *Nature* **2006**, *442*, 282–286.

[5] Dikin, D. A.; Stankovich, S.; Zimney, E. J.; Piner, R. D.; Dommett, G. H. B.; Evmenenko, G.; Nguyen, S. T.; Ruoff, R. S. Preparation and characterization of graphene oxide paper. *Nature* **2007**, *448*, 457–460.

[6] Li, D.; Müller, M. B.; Gilje, S.; Kaner, R. B.; Wallace, G. G. Processable aqueous dispersions of graphene nanosheets. *Nat. Nanotechol.* **2008**, *3*, 101–105.

[7] Hummers, W. S.; Offeman, R. E. Preparation of graphitic oxide. *J. Am. Chem. Soc*. **1958**, *80*, 1339.

[8] Cai, D. Y.; Song, M. Preparation of fully exfoliated graphite oxide nanoplatelets in organic solvents. *J. Mater. Chem*. **2007**, *17*, 3678–3680.

[9] Hontoria-Lucas, C.; Lopez-Peinado, A. J.; Lopez-Gonzalez, J. D. D.; Rojas-Cervantes, M. L.; Martin-Aranda, R. M. Study of oxygen-containing groups in a series of graphite oxides: Physical and chemical characterization. *Carbon* **1995**, *33*, 1585–1592.

[10] Szabo, T.; Berkesi, O.; Dekany, I. DRIFT study of deuterium-exchanged graphite oxide. *Carbon* **2005**, *43*, 3186–3189.

[11] Hermanson, G. T. *Bioconjugate Techniques*; Academic Press: San Diego, 1996; Ch2.

[12] Stankovich, S.; Piner, R. D.; Nguyen, S. T.; Ruoff, R. S. Synthesis and exfoliation of isocyanate-treated graphene oxide nanoplatelets. *Carbon* **2006**, *44*, 3342–3347.

[13] Reed, B. W.; Sarikaya, M. Electronic properties of carbon nanotubes by transmission electron energy-loss spectroscopy. *Phys. Rev. B* **2001**, *64*, 195404.

[14] Attal, S.; Thiruvengadathan, R.; Regev, O. Determination of the concentration of single-walled carbon nanotubes in aqueous dispersions using UV-visible absorption spectroscopy. *Anal. Chem*. **2006**, *78*, 8098–8104.

[15] Cherukuri, P.; Bachilo, S. M.; Litovsky, S. H.; Weisman, R. B. Near-infrared fluorescence microscopy of single-walled carbon nanotubes in phagocytic cells. *J. Am. Chem. Soc*. **2004**, *126*, 15638–15639.

[16] Welsher, K.; Liu, Z.; Daranciang, D.; Dai, H. Selective probing and imaging of cells with single walled carbon nanotubes as near-infrared fluorescent molecules. *Nano Lett*. **2008**, *8*, 586–590.

[17] Price, C. A. *Centrifugation in Density Gradients;* Academic Press: New York, 1982; Ch. 5.

[18] Sun, X. M.; Zaric, S.; Daranciang, D.; Welsher, K.; Lu, Y. R.; Li, X. L.; Dai, H. J. Optical properties of ultrashort semiconducting single-walled carbon nanotube capsules down to sub-10 nm. *J. Am. Chem. Soc*. **2008**, *130*, 6551–6555.

[19] Lerf, A.; He, H. Y.; Forster, M.; Klinowski, J. Structure of graphite oxide revisited. *J. Phys. Chem. B* **1998**, *102*, 4477–4482.

[20] Sun, Y. P.; Zhou, B.; Lin, Y.; Wang, W.; Fernando, K. A. S.; Pathak, P.; Meziani, M. J.; Harruff, B. A.; Wang, X.; Wang, H. F.; Luo, P. J. G.; Yang, H.; Kose, M. E.; Chen, B. L.; Veca, L. M.; Xie, S. Y. Quantum-sized carbon dots for bright and colorful photoluminescence. *J. Am. Chem. Soc.* **2006**, *128*, 7756–7757.

[21] Liu, H. P.; Ye, T.; Mao, C. D. Fluorescent carbon nanoparticles derived from candle soot. *Angew. Chem. Int. Ed*. **2007**, *46*, 6473–6475.

[22] Kam, N. W. S.; Liu, Z. A.; Dai, H. J. Carbon nanotubes as intracellular transporters for proteins and DNA: An investigation of the uptake mechanism and pathway. *Angew. Chem. Int. Ed*. **2006**, *45*, 577–581.

[23] Aubin, J. E. Autofluorescence of viable cultured mammalian cells. *J. Histochem. Cytochem*. **1978**, *27*, 36–43.

[24] Tsyboulski, D. A.; Rocha, J. D. R.; Bachilo, S. M.; Cognet, L.; Weisman, R. B. Structure-dependent fluorescence efficiencies of individual single-walled carbon nanotubes. *Nano Lett.* **2007**, *7*, 3080–3085.

[25] Carlson, L. J.; Maccagnano, S. E.; Zheng, M.; Silcox, J.; Krauss, T. D. Fluorescence efficiency of individual carbon nanotubes. *Nano Lett*. **2007**, *7*, 3698–3703.

[26] Crochet, J.; Clemens, M.; Hertel, T. Quantum yield heterogeneities of aqueous single-wall carbon nanotube suspensions. *J. Am. Chem. Soc.* **2007**, *129*, 8058–8059.

[27] Liu, Z.; Sun, X. M.; Nakayama-Ratchford, N.; Dai, H. J. Supramolecular chemistry on water-soluble carbon nanotubes for drug loading and delivery. *ACS Nano* **2007**, *1*, 50–56.